



Research paper

Graphene quantum dots modified mesoporous graphite carbon nitride with significant enhancement of photocatalytic activity



Jinyuan Liu^a, Hui Xu^{a,*}, Yuanguo Xu^a, Yanhua Song^c, Jiabiao Lian^a, Yan Zhao^a, Liang Wang^{b,*}, Liying Huang^a, Haiyan Ji^a, Huaming Li^{a,*}

^a School of the Environment and Safety Engineering, Institute for Energy Research, Jiangsu University, Zhenjiang 212013, PR China

^b Institute of Nanochemistry and Nanobiology, Shanghai University, Shanghai 200444, PR China

^c School of Environmental and Chemical Engineering, Jiangsu University of Science and Technology, Zhenjiang 212003, PR China

ARTICLE INFO

Article history:

Received 23 August 2016

Received in revised form 1 January 2017

Accepted 24 January 2017

Available online 25 January 2017

Keywords:

GQDs/mpg-C₃N₄ composites

Photocatalytic activity

Visible light

ABSTRACT

Hydroxyl-graphene quantum dots (GQDs) modified mesoporous graphitic carbon nitride (mpg-C₃N₄) composites were fabricated through electrostatic interactions. A variety of techniques were applied to discuss systematic effect on the morphology, optical, electronic properties and structure of GQDs/mpg-C₃N₄ composites. Remarkably, the 0.5 wt% GQDs/mpg-C₃N₄ composites exhibited higher photocatalytic activity than that of the pure mpg-C₃N₄ by using rhodamine B (RhB) and colorless tetracycline hydrochloride (TC) as pollutants under visible light irradiation. The results indicated that uniform dispersion of GQDs on the surface of mpg-C₃N₄ and intimate contact between the two materials contributed to the enhanced activity. Radical trapping experiments and electron spin resonance tests both certified that the GQDs/mpg-C₃N₄ composites can generate more •O₂⁻ species and a small fraction of holes for photocatalytic degradation.

© 2017 Elsevier B.V. All rights reserved.

1. Introduction

The ever growing energy crisis has led to repaid increase in research and development in energy conversion and storage field. However, along with that it has also increased the hazardous impacts on environment. Hence a considerable amount of attention has been shifted toward lowering catastrophic impacts on environment, photocatalysis being one. For the organic pollutants contaminating the water bodies photocatalysis are highly effective. Developing of new visible-light active photocatalysts with abundant, stable materials showing efficient, high activity performance is a key point [1,2]. As a novel class of carbon nitride, melon-based graphitic carbon nitride (g-C₃N₄) is a fascinating π -conjugated semiconductor with suitable electronic structure (band gap = 2.7 eV) [3–6]. Also low cost, easy availability, high stability, non-toxic as well as easily tailor-able structure make g-C₃N₄ a promising candidate in photocatalytic application [7–11]. Nevertheless, a small specific surface area leading to the rapid recombination of photoinduced electron-holes pairs and insufficient solar-light absorption, inhibit its further practical

applications. Among the approaches reported emphasis is given to synthesize the modified g-C₃N₄ photocatalysts [12,13], including doping with nonmetal and metals species, like B, F [14], K [15], Br [16], I [17], P [18], Fe [19] and Au [20]. In addition, fabrication of g-C₃N₄-based heterojunction with secondary semiconductors or co-catalysts is also used to increase migration of photo-generated electron [21–25]. The other approach is to fabricate different morphologies g-C₃N₄ nanospheres [24,26], nanosheets [27–30], nanotubes [31], nanorods [32], helical [33] or seaweed [34] rendering enlarged specific surface area for enhanced photocatalytic activity.

Mesoporous materials are more attractive due to the outstanding properties and potential applications. Mesoporous TiO₂ [35], Co₃O₄ [36,37] and WO₃ [38] have exhibited well properties in the field of fuel cells, lithium ion batteries, supercapacitor, photocatalytic degradation of organic pollutions, gas storage and separation and dye sensitized solar cells [39–43]. Especially, non-metal nanomaterials, like carbonaceous and carbon nitride nanomaterials, with highly stable and less expensive earth-abundant elements have attracted much attention. Graphitic carbon nitride with mesoporous structure is beneficial to increase the photocatalytic performance due to the enhancing the light harvesting ability and the adsorption capability [44]. Meanwhile, based on the pore structure, it is crucial to further boost the photocatalytic activity of

* Corresponding authors.

E-mail addresses: xh@ujs.edu.cn (H. Xu), wangl@shu.edu.cn (L. Wang), lihm@ujs.edu.cn (H. Li).

pure mpg-C₃N₄ by combining a small amount of metal and non-metal oxide, including Co₃O₄/mpg-C₃N₄ [45], ZnO/mpg-C₃N₄ [46], TiO₂/mpg-C₃N₄ [47], PW₁₂/mpg-C₃N₄ [48] and WO₃/mpg-C₃N₄ [49]. These composites have been demonstrated to be capable of remarkably enhancing the photocatalytic activity. However, the object of research in carbon nitride material is to further explore co-catalysts as less expensive and stable performance. Therefore, carbonaceous is no doubt becoming as one of the most popular materials, like graphene, graphene oxide, carbon nanotubes and novel graphene quantum dot materials. Graphene quantum dots (GQDs), as a family of quantum dots materials, has currently aroused increasing attention [50–57]. GQDs with edge-enriched and small size usually possess unique character compared to other carbon materials [58–62].

Herein, we designed GQDs/mpg-C₃N₄ materials via a facile approach to solve the limitation of pristine mpg-C₃N₄. The as-prepared GQDs/mpg-C₃N₄ composites were obtained through electrostatic attraction between mpg-C₃N₄ and GQDs in ethanol solution. To the best of our knowledge, there is no report on the fabrication strategy of GQDs/mpg-C₃N₄ by electrostatic attraction. In this study, the electrostatic interaction is as a promising method to solve problem of aggregation and contact. The morphology, structure and optical/electric properties of GQDs/mpg-C₃N₄ were evaluated by various physicochemical techniques. The results indicated that the GQDs/mpg-C₃N₄ composites exhibited much higher visible-light performance than pristine mpg-C₃N₄ due to the incorporation of GQDs.

2. Experimental section

2.1. Preparation of photocatalysts

All chemicals were of analytically grade. The GQDs were synthesized according to the papers through an alkali-catalyzed water-phase molecular fusion method [63].

2.1.1 Preparation of OH-functionalized GQDs

Hydroxyl-functionalized GQDs were synthesized according to our previous work [63,64]. In this synthesis procedure, 2 g pyrene was nitrated into trinitropyrene in hot HNO₃ at 80 °C under refluxing and stirring for 12 h. After cooled to room temperature, the mixture was dissolved in distilled water and filtered through a 0.22 μm microporous membrane to remove to acid. The resultant yellow trinitropyrene was dispersed in 0.2 M NaOH by ultrasonication for 2 h. The suspension was transferred to a 100 mL Teflon-lined stainless steel autoclave for 10 h at 200 °C. After cooling, the water-soluble GQDs were obtained through 0.22 μm microporous membrane to remove impurities (insoluble carbon products). The purified black GQDs were dissolved in distilled water.

2.1.2 Preparation of mpg-C₃N₄

The pure mpg-C₃N₄ was synthesized using SiO₂ as hard template [65–67]. Firstly, cyanamide was added in silica colloidal solution (mass ratios, cyanamide: template = 0.5). The mixture solution was stirred at room temperature for 4 h and heated at 60 °C for 2 h to get transparent gel. The resulting gel was heated to 550 °C in N₂ flow at a rate of 2.3 °C/min, dwelling for 4 h. The silica template was removed by NH₄HF₂. The sample was separated by centrifuging, washing with ultrapure water and ethanol.

2.1.3 Synthesis of GQDs/mpg-C₃N₄ composites

The GQDs/mpg-C₃N₄ composites were synthesized as follows. Firstly, an appropriate amount of mpg-C₃N₄ was dissolved into 15 mL ethanol and sonicated for 30 min to obtain a homogeneous suspension. Then, a certain concentration GQDs solution

was dispersed in the above solution and stirred for 12 h. After ethanol vaporization, the powder was obtained after drying at 80 °C. GQDs/mpg-C₃N₄ photocatalysts with different GQDs content designated as X wt% GQDs/mpg-C₃N₄, wherein "X" represent the mass percentage of GQDs (X = 0.1, 0.2, 0.5, 1, 2 and 3 wt%).

2.2. Characterization of materials

The crystal structures of photocatalysts were recorded by X-ray diffraction (XRD) using Shimadzu XRD-6000 with Cu Kα radiation in the range of 2θ from 10° to 80°. The chemical environment of as-prepared photocatalysts were analyzed by X-ray photoelectron spectroscopy (XPS) using VG MultiLab 2000 system with a monochromatic Mg-Kα source operated at 20 kV. The nitrogen adsorption-desorption isotherms (TriStar II 3020) was used to calculate surface area and pore size of as-prepared samples in the relative pressure range of 0.1–0.9. Transmission electron microscopy (TEM) images of all samples were performed on JEOL JEM-2010 (200 kV). The Z-potential was carried out on the Malvern Zetasizer Nano-S90 (England). Diffuse reflection spectra (DRS) was acquired on Shimadzu UV-2450 spectrophotometer in the range of 200–800 nm (BaSO₄ as reference material). Composition analysis of as-prepared materials were carried on the Fourier transforms infrared spectra (FT-IR) using Nicolet Nexus 470 spectroscopy. The photoluminescence spectra of as-prepared materials were monitored on a QuantaMaster & TimeMaster Spectrofluorometer (excitation wavelength at 360 nm). Electron spin resonance (ESR) spectra was conducted on a Bruker model ESR JES-FA200 spectrometer.

2.3. Photocatalytic activity measurements

The photocatalytic performance of GQDs/mpg-C₃N₄ samples was investigated using 10 mg/L RhB and 20 mg/L TC as pollutants. 25 mg and 50 mg GQDs/mpg-C₃N₄ composites were dispersed in the Pyrex photocatalytic reactors including 50 mL RhB dye and colorless TC, respectively. Photocatalytic reaction apparatus with 300 W Xe arc lamp was used as light source with a filter ($\lambda > 400$ nm) to provide the visible light. The photocatalytic experiments were performed at constant temperature by a circulating water system. Prior to light irradiation, the suspension was stirred for 30 min without light to reach adsorption and desorption equilibrium, and this adsorption equilibrium point is the starting point of photocatalytic reaction. During the photoreaction process, 3 mL suspension was collected at 30 min intervals and centrifuged. The decay of absorbance of organic dye RhB and TC were analyzed by an UV-vis spectrophotometer at wavelength 553 nm and 356 nm, respectively.

2.4. Photoelectrochemical measurements

Photocurrent measurements were carried out a CHI 660B electrochemical workstation (Chenhua Instrument), including a standard three electrodes system configuration with a platinum wire as counter electrode, an Ag/AgCl wire (saturated KCl solution) as reference electrode, and 0.1 M Na₂SO₄ solution as the electrolyte. The working electrode was prepared as followed: 5 mg of sample was dispersed in 1 mL ethylene glycol solution. The suspension was then spread on a 3 cm × 1 cm ITO glass substrate with an active area of about 0.5 cm × 1 cm and dried under infrared lamp to form mpg-C₃N₄ and GQDs/mpg-C₃N₄ modified ITO electrodes. 500 W Xe lamp was used as light source.

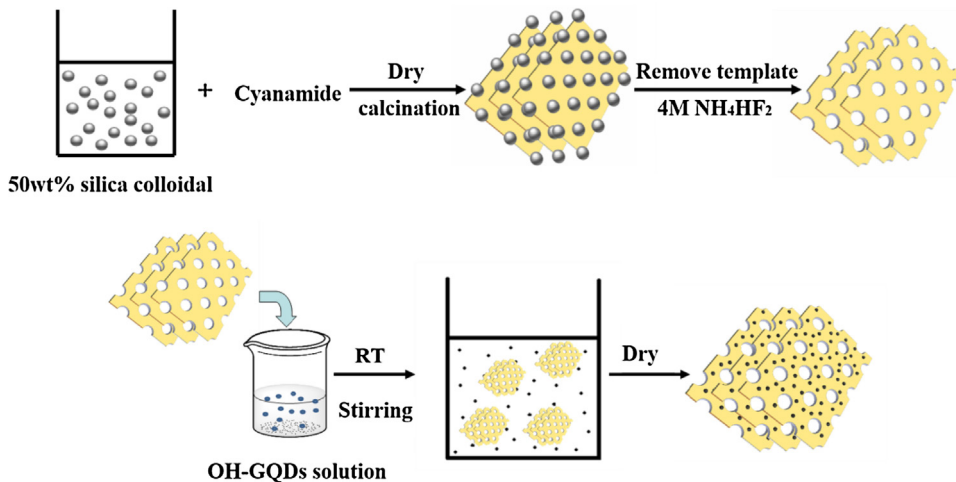


Fig. 1. Schematic for the synthesis process of GQDs/mpg-C₃N₄ by electrostatic attraction.

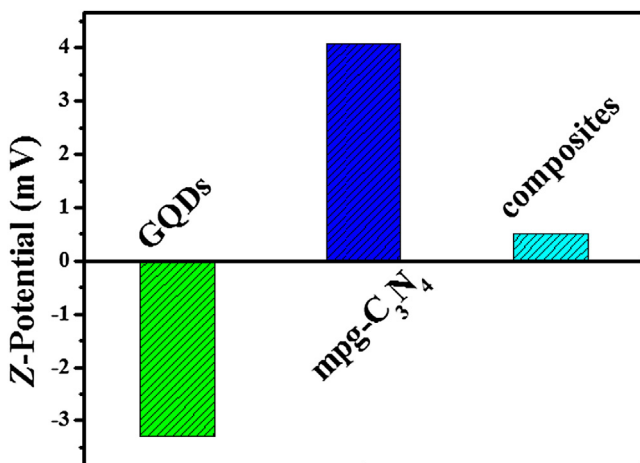


Fig. 2. Z-potential of mpg-C₃N₄, GQDs and GQDs/mpg-C₃N₄ in ethanol solution.

3. Results and discussion

3.1. The proposed formation process of GQD/mpg-C₃N₄

For the synthesis of GQDs/mpg-C₃N₄ with different mass ratios, a general electrostatic interactions method was introduced to fabricate a homogeneous solution, as shown in Fig. 1. To investigate the formation process of composites, electrostatic attraction of two materials was tested by the Z-potential apparatus and the results were shown in Fig. 2. Z-potential of mpg-C₃N₄ was 4.07 mV due to the use of NH₄HF₂ as etchant, indicating that etching process rendered mpg-C₃N₄ positive charge on surface. In comparison to mpg-C₃N₄, Z-potential of GQDs was -3.28 mV, suggesting negative polarity. Therefore, the spontaneous assembly between the negatively charged GQDs and the positively charged mpg-C₃N₄ was achieved. The Z-potential of the GQDs/mpg-C₃N₄ was decreased to 0.5 eV, indicating that GQDs successfully adsorbed on the surface of multilayer mpg-C₃N₄ sheets. Owing to electrostatic attraction between mpg-C₃N₄ and GQDs, it is beneficial for the homogenous dispersion of GQDs. The above results are further confirmed by TEM investigation. As shown in Fig. 3a, the TEM images of GQDs exhibited uniformly size about 5 nm. The Fig. 3b shows that the GQDs are well dispersed with uniform lateral sizes. The average size of GQDs determined by TEM is about 5 nm. The Fast Fourier Transformation (FFT) pattern show that the GQDs are almost defect-free graphene single crystals (Fig. 3c). Many spherical pores with a mean diameter

of about 20 nm were observed on the surface of the mpg-C₃N₄ (Fig. 3d and e), suggesting that the holes of mpg-C₃N₄ successfully copied by HS-40 colloidal solution. After introduction of the GQDs into mpg-C₃N₄, 0.5 wt% GQDs/mpg-C₃N₄ composites have the similar porosity structure comparison to the pure mpg-C₃N₄ (Fig. 3f). Meanwhile, the GQDs easily combine with mpg-C₃N₄ and disperse well via electrostatic attraction [68,69].

3.2. XRD and FT-IR analysis

The structural characteristics of as-prepared mpg-C₃N₄ and GQDs/mpg-C₃N₄ with the different mass ratios of GQDs were measured by XRD technique (Fig. 4a). The pure mpg-C₃N₄ displays two distinct diffraction peaks at 13.0° (100) reflection and 27.4° (002), which indicated the characteristic graphitic-like layered stacking of CN-based materials. Nevertheless, there was no characteristic peak attributed to GQDs, which may due to the low GQDs content and high dispersion in as-prepared GQDs/mpg-C₃N₄ composites. It also found that the GQDs modification has no significant effect on the layer-shaped structure of mpg-C₃N₄. Fig. 4b presents FT-IR spectra of GQDs/mpg-C₃N₄ samples. The pure mpg-C₃N₄ exhibited characteristic FT-IR peaks similar to the previous reports [48]. The peaks from 3000 to 3600 cm⁻¹ are assigned to N–H groups originated from the incomplete condensation or the residual hydrogen atoms bound to the edges of the graphite-like CN. The s-triazine ring mode at 808 cm⁻¹ and stretching vibration modes in the regions of 1200–1650 cm⁻¹ belongs to C=N and C–N heterocycles. However, the characteristic signal C–OH of OH-GQDs at 1270 cm⁻¹ not detected in the FT-IR spectrum, which is mainly due to strong stretching vibration of C–N.

3.3. XPS analysis

XPS is employed to determine the chemical states and characterize the intimate interaction between GQDs and mpg-C₃N₄. Fig. 5a shows the survey XPS spectra of pure mpg-C₃N₄ and 0.5 wt% GQDs/mpg-C₃N₄, indicating the presence of carbon, nitrogen and oxygen. In Fig. 5b, high-resolution C 1s spectra of pure mpg-C₃N₄ can be de-convoluted into two species: C=C (284.6 eV) and sp²-hybridized carbon in N=C–N₂= (288.2 eV), whereas the peak of GQDs/mpg-C₃N₄ at 285.9 eV is assigned to C–OH of GQDs [70], demonstrating the co-existence of GQDs and mpg-C₃N₄ in the composites attributed to spontaneous self-assembly between GQDs and mpg-C₃N₄. Fig. 5c presents high-resolution N 1s spectrum with four species peaks at 398.7 eV, 399.8 eV, 401.0 eV and 404.4 eV,

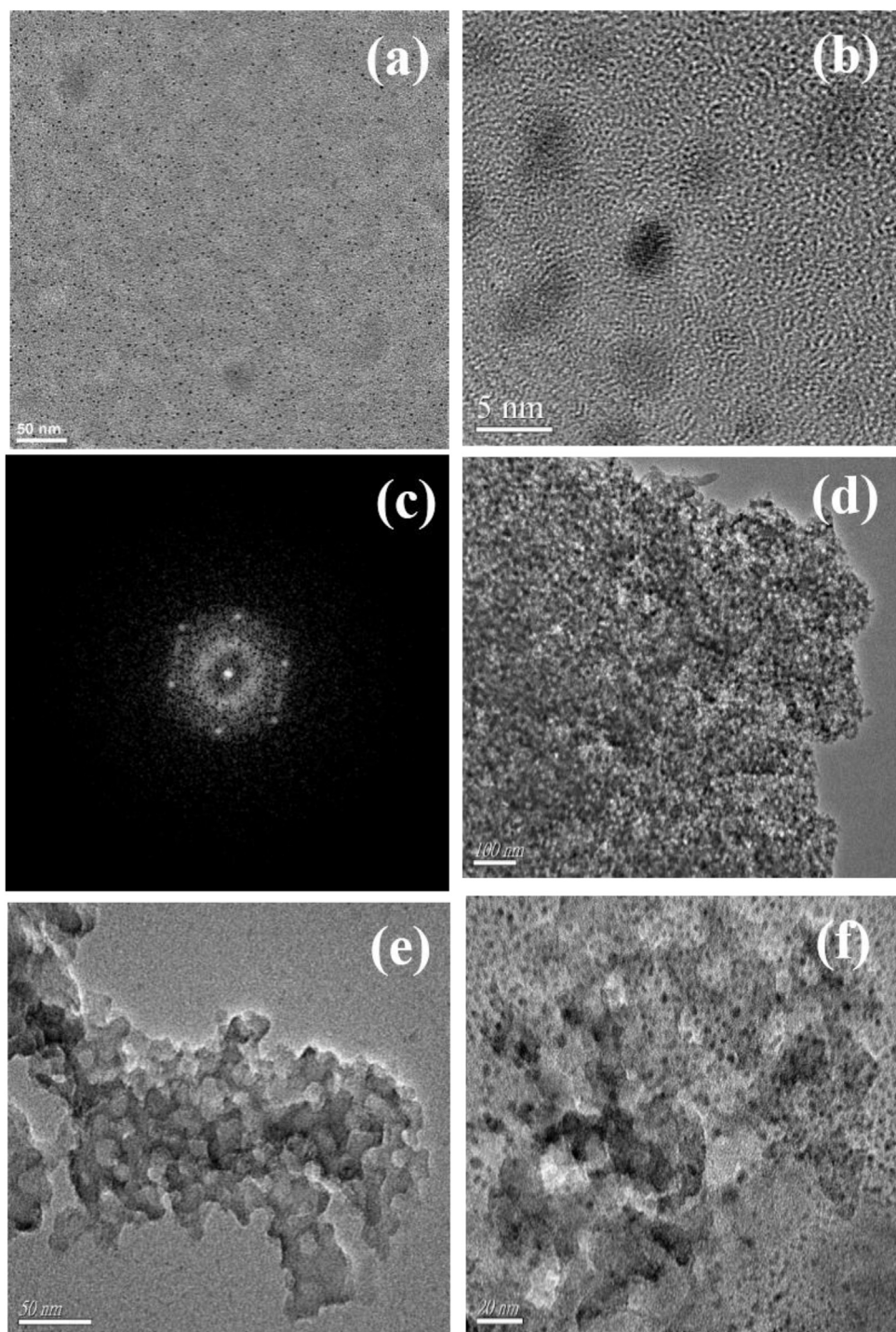


Fig. 3. TEM images (a, b) and Fast Fourier Transformation (FFT) pattern (c) of GQDs; TEM images of the pure mpg-C₃N₄ (d, e) and 0.5 wt% GQDs/mpg-C₃N₄ composites (f).

respectively. The signal peak at 398.7 eV is attributed to electrons originated from sp²-hybridized nitrogen atoms in C=N—C, which is in good agreement the FT-IR analysis. While two main peaks at 399.8 eV and 401.0 eV are attributed to the tertiary nitrogen (N-(C)₃) and the amino functions carrying hydrogen (C—N—H) of pure mpg-C₃N₄, which correspond to structural defects and incomplete condensation in the process of cyanamide polycondensation. The weak peak at 404.4 eV may be assigned to π -excitation. From the high-resolution XPS spectrum of O 1s (Fig. 5d), the peak of pure mpg-C₃N₄ at 531.3 eV is assigned to O—H, while appear a new peak at 533.2 eV for GQD/mpg-C₃N₄ sample, revealing the presence of

C—OH. All above results further confirmed the formation of samples composed of mpg-C₃N₄ and GQDs, suggesting the GQDs have been introduced into the multilayer mpg-C₃N₄ sheets successfully.

3.4. BET and BJH analysis

The nitrogen adsorption-desorption isotherms of 0.5 wt% GQDs/mpg-C₃N₄ and mpg-C₃N₄ are shown in Fig. 6. For the pure mpg-C₃N₄, the physical adsorption isotherms show a typical IV with a distinct H1 hysteresis loop observed in the range of 0.6–1.0 P/P_0 , which is characteristic of mesoporous structure.

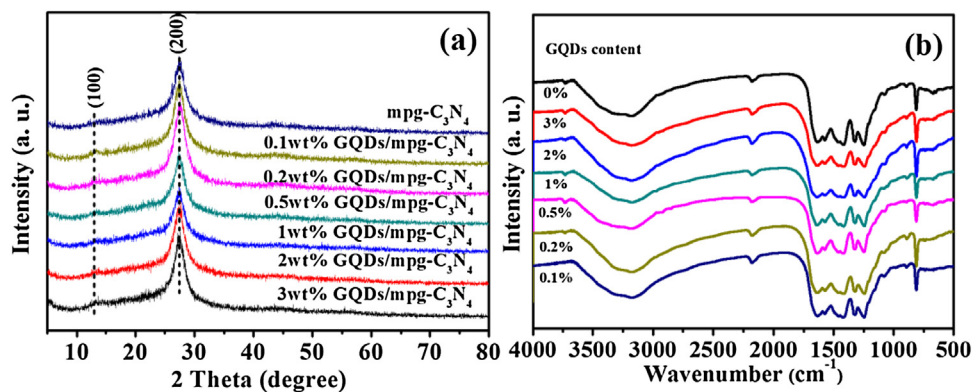


Fig. 4. XRD (a) and FT-IR (b) patterns of mpg-C₃N₄ and GQDs/mpg-C₃N₄ with different contents of GQDs.

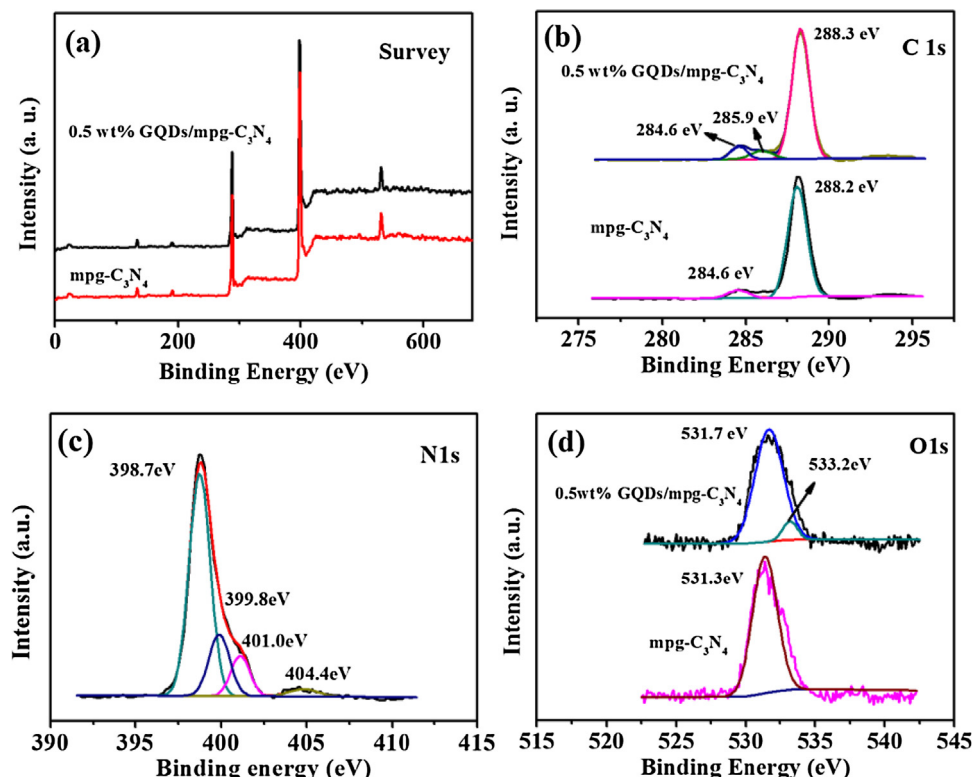


Fig. 5. XPS spectra of mpg-C₃N₄ and 0.5 wt% GQDs/mpg-C₃N₄ sample, survey spectrum (a), C 1s (b), N 1s (c) and O 1s (d).

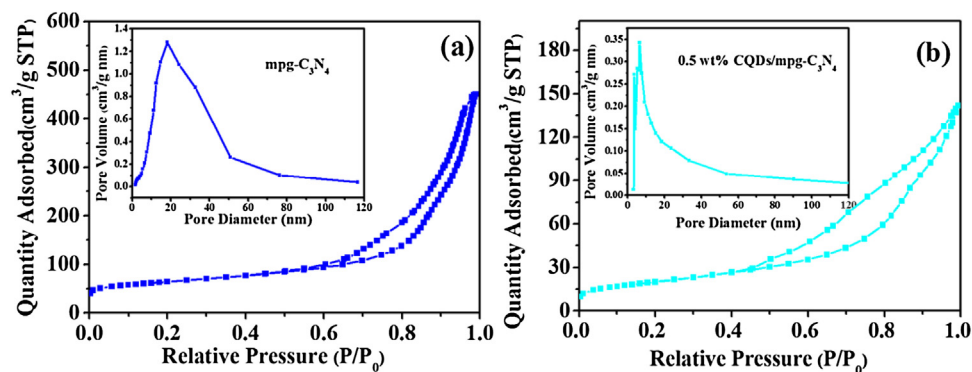


Fig. 6. N₂ adsorption-desorption isotherms and the corresponding pore size distribution curves of pure mpg-C₃N₄ (a) and 0.5 wt% GQDs/mpg-C₃N₄ (b).

After the modification of GQDs, the surface area of composites decreased quickly. The specific surface area of pure mpg-C₃N₄ is 158.07 m²g⁻¹, which was larger than that of 0.5 wt% GQDs/mpg-C₃N₄ (71.3 m²g⁻¹). However, the mesoporous structure of 0.5 wt% GQDs/mpg-C₃N₄ samples still maintained IV type isotherm featuring H1 hysteresis loop at 0.5–1.0 P/P₀, suggesting that mpg-C₃N₄ structure did not damage after incorporating GQDs (Fig. 6b). As shown in Fig. 6a, the appreciable expansion of pore sizes (compared to 12 nm silica template) is found after the replication [71], which may be due to partial hole-wall collapse during the removal of SiO₂ template. It should be noted that the surface area and average pore size of GQDs/mpg-C₃N₄ decreased comparing to pure mpg-C₃N₄, which is mainly due to a part of GQDs blocking the holes of mpg-C₃N₄ [72,73]. As far as we know, the larger surface area is favorable to photocatalytic activity, which is mainly attributed to provide more active sites and adsorb more contaminants on the surface of the photocatalyst.

3.5. Optical and electronic properties

Fig. 7 shows the effect of GQDs on the absorption spectrum of GQDs/mpg-C₃N₄ composites. The pure mpg-C₃N₄ exhibits a fundamental absorption edge at 470 nm. It can be found that mpg-C₃N₄ alone exhibits almost no absorption in the visible region of 470–800 nm. Nevertheless, the light harvesting capability of GQDs/mpg-C₃N₄ composites within the 450 nm to 800 nm gradually improved after modification of GQDs, and thus further to increase photo-generated electron-holes under visible light irradiation, which may be also beneficial to the enhancement of photocatalytic activity.

Photoluminescence techniques are applied to investigate the photo-generated electron-transfer and recombination processes of photo-induced electrons and holes pairs in GQDs, mpg-C₃N₄ and GQDs/mpg-C₃N₄ samples. The PL peak of GQDs at 525 nm can be

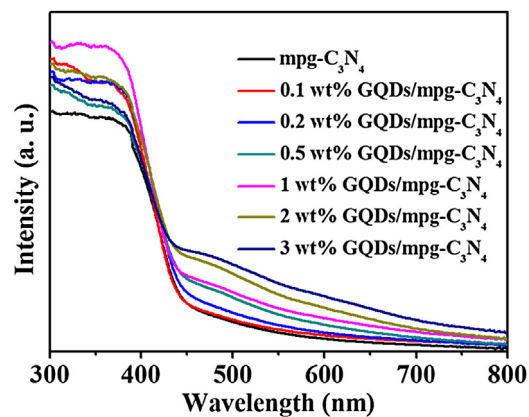


Fig. 7. UV-vis diffuse-reflectance spectra of all samples.

excited in a wide wavelength range (PL, PLE in Fig. 8a). Fig. 8b shows the steady-state PL spectra of the pure mpg-C₃N₄ and GQDs/mpg-C₃N₄. As shown in Fig. 8b, pure mpg-C₃N₄ (excited at 360 nm) has a strong emission peak centered at about 467 nm. After the modification of GQDs, the emission intensity of GQDs/mpg-C₃N₄ material decreased significantly, revealing higher separation efficiency of photo-excited charge and holes.

3.6. Photocatalytic tests

The photocatalytic performance of composites was mainly evaluated by photo-degradation of RhB. Blank experiment was carried out without any photocatalyst. The degradation efficiency was not changed, suggesting that the direct photolysis of RhB can be negligible under visible-light illumination. Fig. 9a presents efficiency for pure mpg-C₃N₄, 0.1, 0.2, 0.5, 1, 2 and 3 wt% GQDs/mpg-C₃N₄

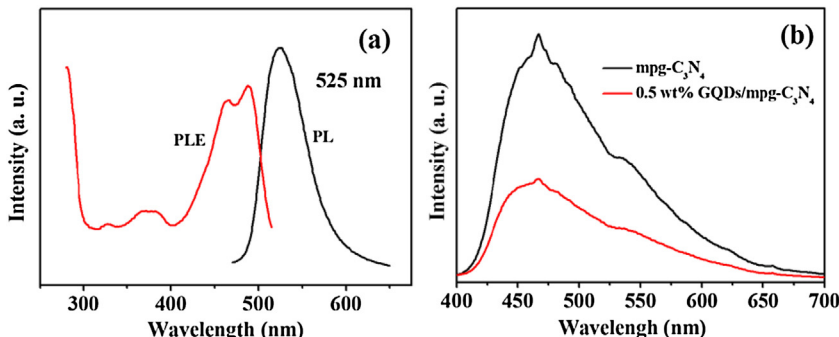


Fig. 8. PL and excitation (PLE) spectra of GQDs (a); photoluminescence spectra of pure mpg-C₃N₄ and 0.5 wt% GQDs/mpg-C₃N₄ (b).

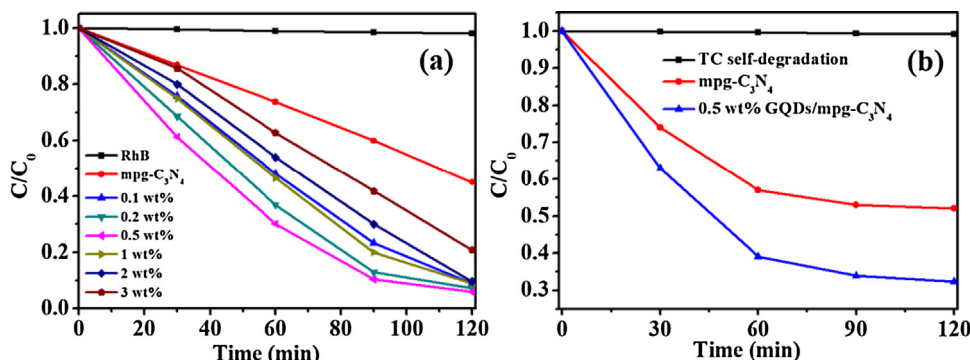


Fig. 9. Photocatalytic activity of RhB in the presence of the GQDs/mpg-C₃N₄ composites with different contents of GQDs under visible light irradiation (a); photocatalytic activity of TC in the presence of mpg-C₃N₄ and 0.5 wt% GQDs/mpg-C₃N₄ under visible light irradiation (b).

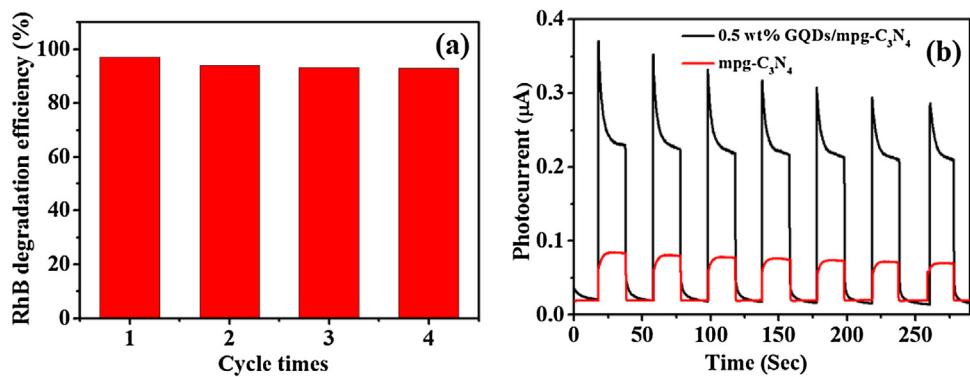


Fig. 10. Cycling runs for the photodegradation of RhB in the presence of 0.5 wt% GQDs/mpg-C₃N₄ under visible light irradiation (a); transient photocurrent response of pure mpg-C₃N₄ and 0.5 wt% GQDs/mpg-C₃N₄ (b).

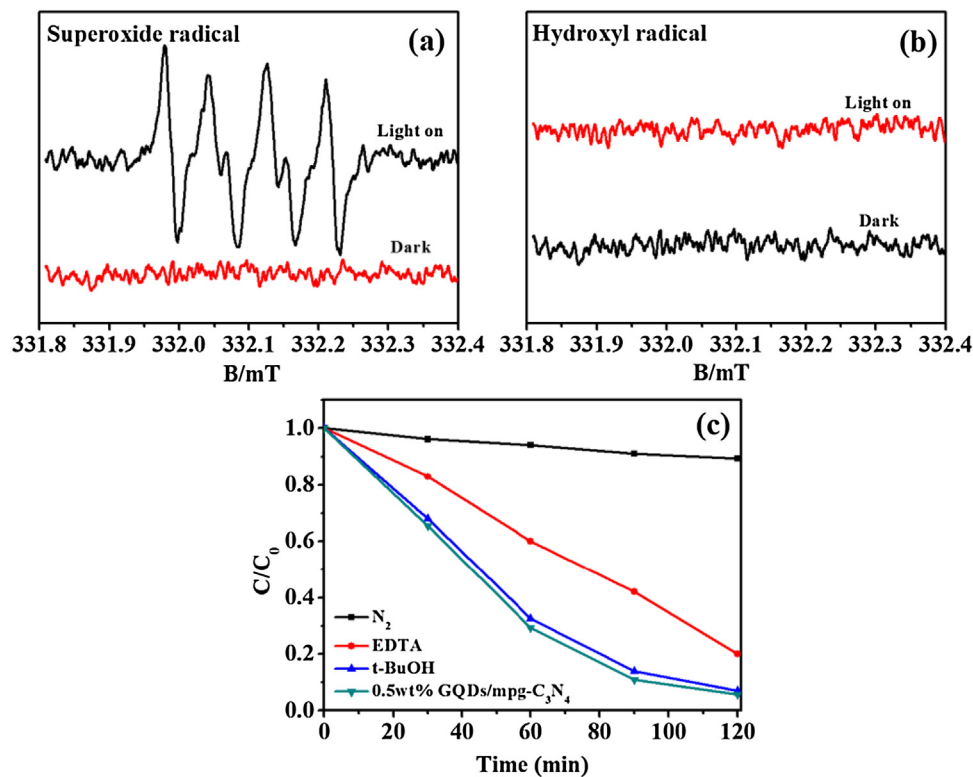


Fig. 11. ESR spectra of radical adducts trapped by DMPO: (a) DMPO-O₂[−] radical species of 0.5 wt% GQDs/mpg-C₃N₄ was detected in methanol, (b) DMPO-OH was used to detect for 0.5 wt% GQDs/mpg-C₃N₄ materials aqueous dispersion; (c) trapping experiment of active species during the photocatalytic degradation of RhB over 0.5 wt% GQDs/mpg-C₃N₄ under visible light irradiation.

samples. As observed in Fig. 9a, the introduction of GQDs have an obviously influence on the photo-degradation efficiency. The 55% RhB could be removed by the pure mpg-C₃N₄, owing to unique mesoporous structure and moderate band gap. For 0.1 wt% GQDs/mpg-C₃N₄ sample, the photocatalytic degradation efficiency was remarkably enhanced. During the GQDs content changed from 0.1 to 0.5 wt%, the photocatalytic activity was further increased. In comparison to the pure mpg-C₃N₄, 0.5 wt% GQDs/mpg-C₃N₄ displayed the highest photocatalytic activity, which had a 42% improvement under visible-light illumination. A further increasing GQDs content caused a rapid reduction for the photocatalytic activity. Although the modification of GQDs were beneficial to charge transfer, too many GQDs cover on the surface of mpg-C₃N₄ would limit the light absorption of mpg-C₃N₄. Therefore, the activity would decrease. To further investigate the photocatalytic degradation of colorless pollutions over GQDs/mpg-C₃N₄ under visible light

irradiation, TC was chosen to evaluate the photocatalytic activity of GQDs/mpg-C₃N₄ composites, and the results were shown in Fig. 9b. It was indicated that the 0.5 wt% GQDs/mpg-C₃N₄ exhibited higher photocatalytic activity than that of pure mpg-C₃N₄. Therefore, it was implied that introduction of GQDs could effectively improve degradation performance of the composites. The stability and reusability of the composites are important factor from the viewpoint of practical applications, and the result is shown in Fig. 10a. After four cycles under uniform conditions, there was no apparent deactivation of the photocatalytic activity over 0.5 wt% GQDs/mpg-C₃N₄, indicating the high stability of 0.5 wt% GQDs/mpg-C₃N₄. The photocurrent tests were conducted for 0.5 wt% GQDs/mpg-C₃N₄ and pure mpg-C₃N₄ in a typical three electrode setup. In Fig. 10b, the higher photocurrent intensity obtained by GQDs/mpg-C₃N₄ could be attributed to the modification of GQDs. The GQDs used as a co-catalyst, promoting the migration efficiency of photo-generated

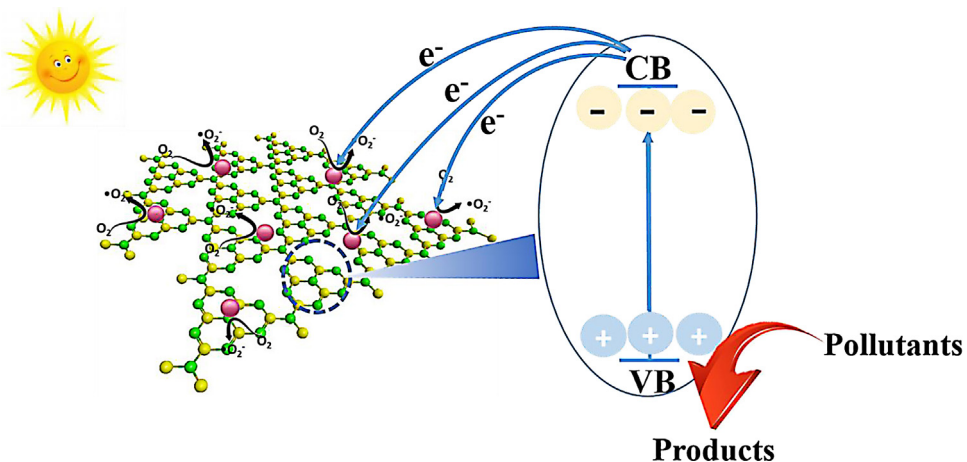


Fig. 12. Schematic model for the photocatalytic mechanism of GQDs/mpg-C₃N₄ composites.

electrons. To sum up, the presence of synergistic effect between GQDs and mpg-C₃N₄ facilitates the photo-generated electron from mpg-C₃N₄ to GQDs, resulting in enhanced photocatalytic activity over GQDs/mpg-C₃N₄.

3.7. Possible reaction mechanism

In order to investigate the possible reactive species, ESR tests were used in the photoreaction process of GQDs/mpg-C₃N₄ with DMPO in water solution. In Fig. 11a, the GQDs/mpg-C₃N₄ composites were irradiated for 12 min and successfully detected the DMPO-O₂⁻ species in media solution. The results indicated that O₂⁻ was main reactive species under visible light illumination, while no signals were detected without light illumination. As shown in Fig. 11b, no signals of •OH were detected whatever under visible light irradiation or in the dark. Therefore, •OH was not main species in GQDs/mpg-C₃N₄ photocatalytic reaction system.

To further reveal the roles of the main active species on the photoreaction process over GQDs/mpg-C₃N₄ composites, free radicals trapping experiments were tested, and the results were shown in Fig. 11c. The t-BuOH was used as hydroxyl radical scavenger and EDTA-2Na as holes scavenger. Purging N₂ into the solution could make an anaerobic environment, which would prohibit the formation of superoxide radical (•O₂⁻) [74]. The photocatalytic activity of GQDs/mpg-C₃N₄ was slightly inhibited after addition of EDTA-2Na as the holes scavenger, suggesting that holes as active species also taken part in the photodegradation process. When the t-BuOH as electronic quenching agent was added, the photodegradation efficiency of RhB did not obviously reduced, which imply that the •OH was not the main free radicals species. Therefore, the ESR investigation and trapping experiment indicated that •O₂⁻ was active species for this photocatalytic system.

Based on above trapping experiment and ESR results, the possible mechanism schematic of 0.5 wt% GQDs/mpg-C₃N₄ system is presented in Fig. 12. When mpg-C₃N₄ was irradiated under visible light illumination, only a small part of photo-generated electrons participated in photocatalytic reaction process, and the other photo-generated electrons could recombine with holes rapidly. However, in GQDs/mpg-C₃N₄ system, the recombine rate between photo-generated electron and holes was greatly inhibited due to the role of GQDs. The photo-generated electrons from CB of mpg-C₃N₄ sheets could be transferred to GQDs surface quickly, and then generated superoxide. Therefore, the photocatalytic activity was improved.

4. Conclusions

In summary, GQDs/mpg-C₃N₄ composites were prepared utilizing electrostatic attraction. The effects of GQDs contents on the photo-degradation efficiency of RhB dye were investigated. The maximum removal efficiency of RhB reached 97% by using 0.5 wt% GQDs/mpg-C₃N₄ under visible light illumination. Meanwhile, the composites could effectively remove the colorless organic pollutants TC. The high photocatalytic activity of composites was attributed to the introduction of GQDs as electron acceptor. According to the ESR investigation and trapping experiment, •O₂⁻ was the main active species for photo-degradation of pollutants.

Acknowledgements

The authors genuinely appreciate the financial support of this work by the National Nature Science Foundation of China (21476097, 21476098, 21671129), six talent peaks project in Jiangsu Province (2014-JNHB-014).

References

- [1] P. Wang, B.B. Huang, Y. Dai, M.H. Whangbo, *Phys. Chem. Chem. Phys.* 14 (2012) 9813–9825.
- [2] D. Chatterjee, S. Dasgupta, *J. Photochem. Photobiol. C* 6 (2005) 186–205.
- [3] Q.J. Xiang, J.G. Yu, M. Jaroniec, *J. Phys. Chem. C* 115 (2011) 7355–7363.
- [4] Y. Wang, X.C. Wang, M. Antonietti, *Angew. Chem. Int. Ed.* 51 (2012) 68–69.
- [5] S.C. Yan, Z.S. Li, Z.G. Zou, *Langmuir* 5 (2009) 10397–10401.
- [6] J.S. Zhang, M.W. Zhang, L.H. Lin, X.C. Wang, *Angew. Chem. Int. Ed.* 54 (2015) 1–6.
- [7] Y. Zheng, J. Liu, J. Liang, M. Jaroniec, S.Z. Qiao, *Energy Environ. Sci.* 5 (2012) 6717–6731.
- [8] X.C. Wang, K. Maeda, A. Thomas, K. Takanabe, G. Xin, J.M. Carlsson, K. Domen, M. Antonietti, *Nat. Mater.* 8 (2009) 76–80.
- [9] Y. Zhang, L.H. Lin, B. Wang, X.C. Wang, *Angew. Chem. Int. Ed.* 54 (2015) 12868–12884.
- [10] J.N. Qin, S.B. Wang, H. Ren, Y.D. Hou, X.C. Wang, *Appl. Catal. B: Environ.* 179 (2015) 1–8.
- [11] G.G. Zhang, Z.A. Lan, X.C. Wang, *Angew. Chem. Int. Ed.* (2016), 10.1002/anie.201607375.
- [12] Z.Z. Lin, X.C. Wang, *Chem. Int. Ed.* 52 (2013) 1735–1738.
- [13] Y.G. Cui, Z.X. Ding, X.Z. Fu, X.C. Wang, *Angew. Chem. Int. Ed.* 51 (2012) 11814–11817.
- [14] Y. Wang, J.S. Zhang, X.C. Wang, M. Antonietti, H.R. Li, *Angew. Chem. Int. Ed.* 49 (2010) 3356–3359.
- [15] M. Zhang, X.J. Bai, D. Liu, J. Wang, Y.F. Zhu, *Appl. Catal. B: Environ.* 164 (2015) 77–81.
- [16] Z.A. Lan, G.G. Zhang, X.C. Wang, *Appl. Catal. B: Environ.* 192 (2016) 116–125.
- [17] G.G. Zhang, M.W. Zhang, X.X. Ye, X.Q. Qiu, S. Lin, X.C. Wang, *Adv. Mater.* 26 (2014) 805–809.
- [18] S.Z. Hu, L. Ma, J.G. You, Z.P. Fan, G. Lu, D. Liu, J.Z. Gui, *Appl. Surf. Sci.* 311 (2014) 164–171.
- [19] X.F. Chen, J.S. Zhang, X.Z. Fu, M. Antonietti, X.C. Wang, *J. Am. Chem. Soc.* 131 (2009) 11658–11659.

[20] D. Yi, X.C. Wang, A. Thomas, M. Antonietti, *ChemCatChem* 2 (2010) 834–838.

[21] K. Sridharan, E. Jang, T.J. Park, *Appl. Catal. B: Environ.* 142 (2013) 718–728.

[22] W.Y. Lu, T.F. Xu, Y. Wang, H.G. Hu, N. Li, X.M. Jiang, W.X. Chen, *Appl. Catal. B: Environ.* 180 (2015) 20–28.

[23] Y.Z. Hong, Y.H. Jiang, C.S. Li, W.Q. Fan, Y. Xu, M. Yan, W.D. Shi, *Appl. Catal. B: Environ.* 180 (2016) 663–673.

[24] D.D. Zheng, G.G. Zhang, X.C. Wang, *Appl. Catal. B: Environ.* 179 (2015) 479–488.

[25] G.G. Zhang, Z.A. Lan, L.H. Lin, S. Lin, X.C. Wang, *Chem. Sci.* 7 (2016) 3062–3066.

[26] D.D. Zheng, X.N. Cao, X.C. Wang, *Angew. Chem. Int. Ed.* 55 (2016) 11512–11516.

[27] H. Xu, J. Yan, X.J. She, L. Xu, J.X. Xia, Y.G. Xu, Y.H. Song, L.Y. Huang, H.M. Li, *Nanoscale* 6 (2014) 1406–1415.

[28] X.J. She, J.J. Wu, J. Zhong, H. Xu, Y.C. Yang, R. Vajtai, J. Lou, Y. Liu, D.L. Du, H.M. Li, P.M. Ajayan, *Nano Energy* 27 (2016) 138–146.

[29] G. Algarra-Siller, N. Severin, S.Y. Chong, T. Bjorkman, R.G. Palgrave, A. Laybourn, M. Antonietti, Y.Z. Khimyak, A.V. Krasheninnikov, J.P. Rabe, *Angew. Chem. Int. Ed.* 53 (2014) 7450–7455.

[30] J.S. Zhang, M.W. Zhang, L.H. Lin, X.C. Wang, *Angew. Chem. Int. Ed.* 54 (2015) 6297–6301.

[31] K. Li, X. Xie, W.D. Zhang, *ChemCatChem* 8 (2016) 2128–2135.

[32] X.J. Bai, L. Wang, R.L. Zong, Y.F. Zhu, *J. Phys. Chem. C* 117 (2013) 9952–9961.

[33] Y. Zheng, L.H. Lin, X.G. Ye, F.S. Guo, X.C. Wang, *Angew. Chem. Int. Ed.* 53 (2014) 11926–11930.

[34] Q. Han, B. Wang, Y. Zhao, C.G. Hu, L.T. Qu, *Angew. Chem. Int. Ed.* 54 (2015) 11433–11437.

[35] T. Wang, L.G. Meng, *Nano Energy* 9 (2014) 50–60.

[36] D. Gu, C.J. Jia, C. Weidenthaler, H.J. Bongard, B. Spliethoff, W. Schmidt, F. Schüth, *J. Am. Chem. Soc.* 137 (2015) 11407–11418.

[37] C.L. Ahn, H.M. Koo, J.M. Jo, H.S. Roh, J.B. Lee, E.J. Jang, J.W. Bae, *Appl. Catal. B: Environ.* 180 (2015) 139–140.

[38] S.H. Baeck, K.S. Choi, T.F. Jaramillo, G.D. Stucky, E.W. McFarland, *Adv. Mater.* 15 (2003) 1269–1273.

[39] M.F. Chen, X.Y. Wang, H.B. Shu, R.Z. Yu, X.Y. Yang, W.H. Huang, *J. Alloy Compd.* 652 (2015) 213–219.

[40] Y.T. Li, Y.T. Pi, L.M. Lu, S.H. Xu, T.R. Ren, *J. Power Sources* 299 (2015) 519–528.

[41] N.S. Sanjini, S. Velmathi, *J. Power Mater.* 22 (2015) 1549–1558.

[42] W.Y. Hong, S.P. Perera, A.D. Burrows, *Microporous Mesoporous Mater.* 214 (2015) 149–155.

[43] J.J. Lu, Z.W. Liu, C.G. Zhu, M. Zhang, M.X. Wan, *Mater. Lett.* 159 (2015) 61–63.

[44] X.F. Chen, J. Young-Si, K. Takanabe, K. Maeda, K. Domen, X.Z. Fu, M. Antonietti, X.C. Wang, *Chem. Mater.* 21 (2009) 4093–4095.

[45] J.D. Hong, S.M. Yin, Y.X. Pan, J.Y. Han, T.H. Zhou, R. Xu, *Nanoscale* 6 (2014) 14984–14990.

[46] D.M. Chen, K.W. Wang, T.Z. Ren, H. Ding, Y.F. Zhu, *Dalt. Trans.* 43 (2014) 13105–13114.

[47] S.S. Ma, J.J. Xue, Y.M. Zhou, Z.W. Zhou, Z.L. Cai, D.B. Zhu, S. Liang, *RSC Adv.* 5 (2015) 64976–64982.

[48] Y.F. Zhu, M.Y. Zhu, L.H. Kang, F. Yu, B. Dai, *Ind. Eng. Chem. Res.* 54 (2015) 2040–2047.

[49] K. Kailasam, A. Fischer, G.G. Zhang, J.S. Zhang, M. Schwarze, M. Schröder, X.C. Wang, S. Reinhard, A. Thomas, *ChemSusChem* 8 (2014) 1404–1410.

[50] P.F. Zhang, Y. Wang, H.R. Li, M. Antonietti, *Green Chem.* 14 (2012) 1904–1908.

[51] L.A. Ponomarenko, F. Schedin, M. Katnelson, R. Yang, E.W. Hill, K.S. Novoselov, A.K. Geim, *Science* 320 (2008) 356–358.

[52] D. Pan, J. Zhang, Z. Li, M. Wu, *Adv. Mater.* 22 (2010) 734–738.

[53] B. Trauzettel, D.V. Bulaev, D. Loss, G. Burkard, *Nat. Phys.* 3 (2007) 192–196.

[54] K.A. Ritter, J.W. Lyding, *Nat. Mater.* 8 (2009) 235–242.

[55] J. Peng, W. Gao, B.K. Gupta, Z. Liu, R. Romero-Aburto, L.H. Ge, L. Song, L.B. Alemany, X.B. Zhan, G.H. Gao, *Nano Lett.* 12 (2012) 844–849.

[56] Y. Li, Y. Hu, Y. Zhao, G.Q. Shi, L.E. Deng, Y.B. Hou, L.T. Qu, *Adv. Mater.* 23 (2011) 776–780.

[57] J.H. Shan, Y.H. Zhu, X.L. Yang, C.Z. Li, *Chem. Commun.* 48 (2012) 3686–3699.

[58] J. Ryu, E. Lee, S. Lee, J. Jang, *Chem. Commun.* 50 (2014) 15616–15618.

[59] B.K. Gupta, G. Kedawat, Y. Agrawal, P. Kumar, J. Dwivedi, S.K. Dhawan, *RSC Adv.* 5 (2015) 10623–10631.

[60] D.Y. Pan, C. Xi, Z. Li, L. Wang, Z.W. Chen, B. Lu, M.H. Wu, *J. Mater. Chem. A* 1 (2013) 3551–3555.

[61] Z.F. Wang, H.D. Zeng, L.Y. Sun, *J. Mater. Chem. C* 3 (2015) 1157–1165.

[62] D. Wang, J.F. Chen, L.M. Dai, *Part. Part. Syst. Char.* 32 (2015) 515–523.

[63] L. Wang, Y.L. Wang, T. Xu, H.B. Liao, C.J. Yao, Y. Liu, Z. Li, Z.W. Chen, D.Y. Pan, L.T. Sun, M.H. Wu, *Nat. Commun.* 5 (2014), <http://dx.doi.org/10.1038/ncomms6357>.

[64] D.Y. Pan, J.K. Jiao, Z. Li, Y.T. Guo, C.Q. Feng, Y. Liu, L. Wang, M.H. Wu, *ACS Sustain. Chem. Eng.* 3 (2015) 2405–2413.

[65] F. Goettmann, A. Fischer, M. Antonietti, A. Thomas, *Angew. Chem. Int. Ed.* 45 (2006) 4467–4471.

[66] A. Thomas, A. Fischer, F. Goettmann, M. Antonietti, J.O. Muller, R. Schloegl, J.M. Carlsson, *J. Mater. Chem.* 18 (2008) 4893–4908.

[67] J.S. Zhang, F.S. Guo, X.C. Wang, *Adv. Fun. Mater.* 23 (2013) 3008–3014.

[68] T.Y. Ma, S. Dai, M. Jaroniec, S.Z. Qiao, *Angew. Chem. Int. Ed.* 53 (2014) 7281–7285.

[69] Y.G. Xu, H. Xu, L. Wang, J. Yan, H.M. Li, Y.H. Song, L.Y. Huang, G.B. Cai, *Dalton Trans.* 42 (2013) 7604–7613.

[70] H. Zhang, L.X. Zhao, F.L. Geng, L.H. Guo, B. Wan, Y. Yang, *Appl. Catal. B: Environ.* 180 (2016) 656–662.

[71] J. Xu, H.T. Wu, X. Wang, B. Xue, Y.X. Li, Y. Cao, *Phys. Chem. Chem. Phys.* 15 (2013) 4510–4517.

[72] A.J. Cai, Q. Wang, Y.F. Chang, X.P. Wang, *J. Alloy Compd.* 692 (2017) 183–189.

[73] J. Di, J.X. Xia, M.X. Ji, B. Wan, S. Yin, Q. Zhang, Z.G. Chen, H.M. Li, *ACS Appl. Mater. Interfaces* 7 (2015) 20111–20123.

[74] B. Wan, J. Di, P.F. Zhang, S. Dai, H.M. Li, *Appl. Catal. B: Environ.* 260 (2017) 127–135.